Real-Time Tendon Strain Estimation of Rotator-Cuff Muscles during Active Robotic-Assisted Rehabilitation

MSc Thesis Report

I.L.Y. Beck

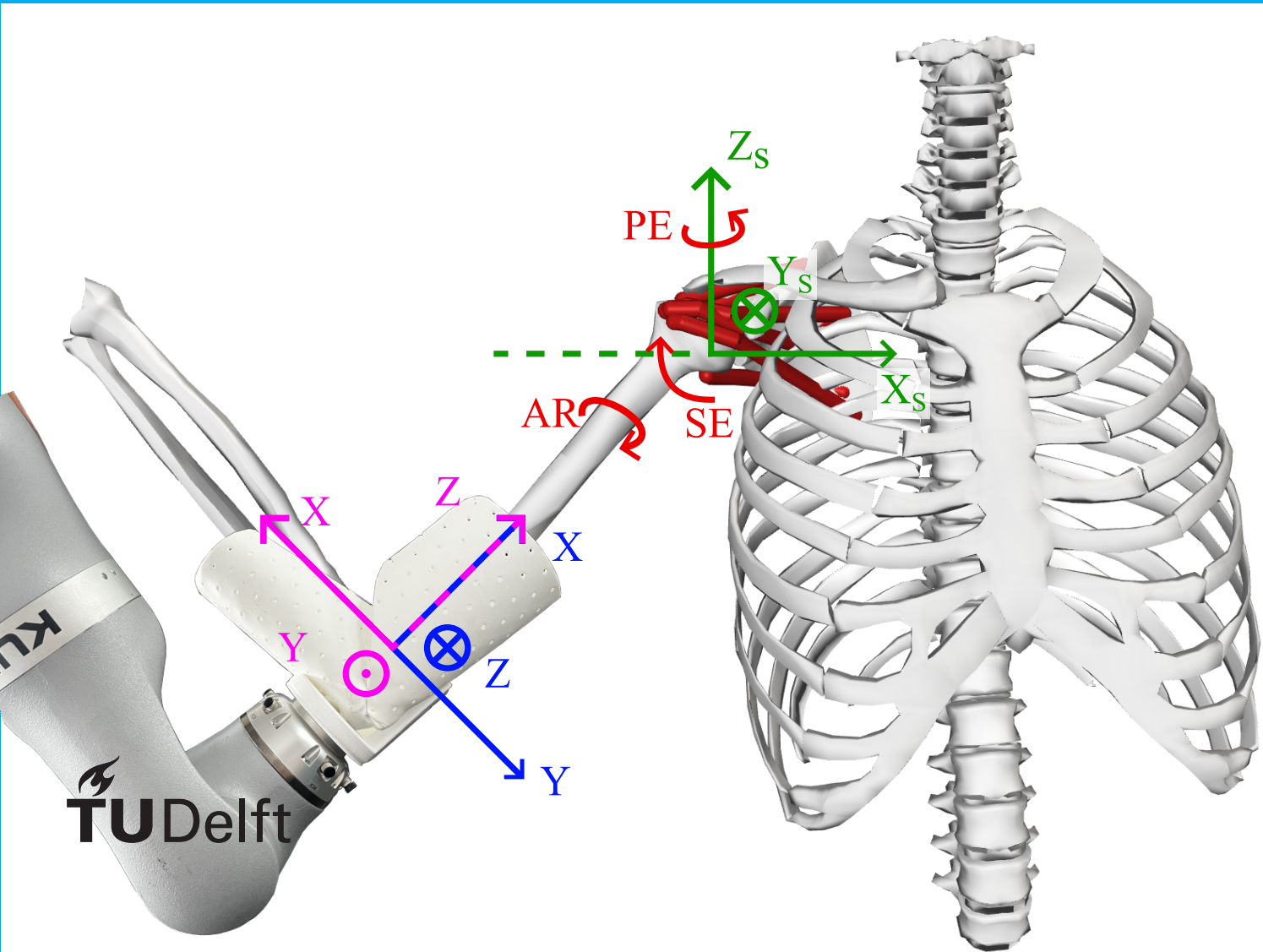

Real-Time Tendon Strain Estimation of Rotator-Cuff Muscles during Active Robotic-Assisted Rehabilitation

by

I.L.Y. Beck

to obtain the degree of

Master of Science
in Mechanical Engineering

At the:
Department of Cognitive Robotics,
Delft University of Technology
to be defended publicly on Friday June 23, 2023 at 10:00 AM.

Student number: 4570839
Supervisors: Dr. A. Seth, TU Delft,
Dr. J.M. Prendergast, TU Delft,
I. Belli, MSc, TU Delft

TU Delft Delft University of Technology

Preface

I hereby proudly present the final fruit of my labor over the past four years in the form of this thesis. After the first six months into my Master's degree, we were faced with a global pandemic, which I used as an excuse to parents to postpone the start of my thesis, and instead, I decided to follow additional courses in many different interesting fields. One of those courses, taught by Ajay Seth, made me end up joining the PTBot group as my graduation project since it combined many parts I enjoyed during my Master's; we had a bit of coding, human movement, and robotics. Again, out of interest and curiosity, I ended up a bit longer in the group than anticipated, but it did help immensely how much fun I had with the team members.

When I started out with my thesis, it was a small team headed by Ajay Seth and Luka Peternel with support from Micah Prendergast. Stephan was doing his thesis on this project on the robotics side, and we had Tom as an honors student from Clinical Technology. Along the way, we picked up Italo Belli as the new Ph.D. candidate, Noah as an honors student from Mechanical Engineering, and as of late, Dinesh and Jevon joined the team. Being surrounded by so many amazing people with different perspectives helped me push myself to be the best possible version I could be.

I am incredibly grateful to the PTbot team, but especially my supervisors: Ajay Seth, J. Micah Prendergast, and Italo Belli. I also want to extend this gratitude to all the friends I made within the CoR department and became an unofficial member of office 34 1-F-480. I'm eternally grateful that you embraced me as one of your own, and in a couple of weeks, I will officially be so! I could not be more excited to return to this environment that made it such a joy to work on my graduation project.

Finally, I could not have done this without the endless support from my parents, brothers, and friends. You've been there for me with emotional support and physical support every time I once again injured myself and provided me with food when you knew I wasn't. Without you, this thesis would not be what it is now.

I.L.Y. Beck
Delft, June 2023

Real-Time Tendon Strain Estimation of Rotator-Cuff Muscles during Active Robotic-Assisted Rehabilitation

Irene Beck[1]
Supervised by: J. Micah Prendergast[2], Italo Belli[1,2], and Ajay Seth[1]

***Abstract*— In this research, we propose a novel method to estimate and monitor rotator cuff tendon strains during active robotic-assisted rehabilitation. Physiotherapists are conservative in the rehabilitation treatment to prevent (re-)injury because they do not know the internal state of the shoulder. By leveraging a robotic device and a musculoskeletal model, our approach provides quantitative information on the risk of re-injury by monitoring the rotator cuff tendon strains. These strains are influenced by the shoulder state and muscle activation, making it crucial to obtain physiologically realistic data on real-time muscle function. To address the muscle redundancy problem, we have developed an innovative algorithm that incorporates constraints on the accelerations, the glenohumeral joint, and the active muscle dynamics. The algorithm's effectiveness was validated through comparisons with electromyography (EMG) measurements. Additionally, we demonstrated the proposed approach using a collaborative robot arm during rehabilitation exercises. The results of our study have yielded new insights into the relationship between the rotator cuff muscles, external forces, and shoulder pose. The findings of our research pave the way for establishing improved therapy that considers the risk of injury to individual muscles and explores a broader range of motion. By providing physiotherapists with valuable quantitative information on rotator cuff tendon strains, our method empowers them to optimize rehabilitation protocols and deliver more personalized and effective care.**

I. Introduction

Disorders of the upper extremity have been reported in 4% to 35% of the general population [1]. Especially the shoulder complex is one of the most common sites for musculoskeletal disorders, with it being the third most common site of pain in the human body [2]. Most of the shoulder complaints (70%) can be attributed to disease of the rotator cuff muscle-tendon units [3]. The rotator cuff complex is comprised of the infraspinatus, supraspinatus, subscapularis, and teres minor muscles. Typical rotator cuff disorders are subacromial pain syndrome and (partial) tendon tears. Tearing of the rotator cuff tendons results primarily in pain and a restricted range of motion of the upper limb. As such, these injuries may result in the inability to perform work in addition to many daily living tasks [4]. Tearing of the rotator cuff tendons has degenerative characteristics, resulting in over 50% aged 60 or older suffering one or more tears [5], [6]. Repetitive overhead activities during work or sports also increase the risk of rotator cuff tears [7]–[9].

Rotator cuff tears are typically treated with either physiotherapy directly or are first surgically repaired, followed by physiotherapy. Effective rehabilitation after surgery is necessary to prevent shoulder joint stiffness, regain range of motion and limit the risk of re-tearing [10]. Regardless of the treatment type, rehabilitation will be time-intensive. Even though rehabilitation should show clinically significant results after twelve weeks [11], patients might be instructed to continue home exercises for as long as six months to a year [12], [13].

The exercises used in conventional rehabilitation programs are often single-degree-of-freedom motions. By only using these exercises, rehabilitation is conservative in the utilized range of motion. Rehabilitation has been limited to these conservative exercises due to the complexity of the shoulder joint and a lack of quantitative insight into the risks of re-tearing, even when assisted by an experienced physiotherapist [14]. The limited range of motion during rehabilitation can delay recovery, whereas moving through a larger range of motion improves recovery [15]. Additionally, current rehabilitation is labor-intensive for the physiotherapist, treating multiple patients with one-on-one manual therapy [16]. Moreover, treatment of the rotator cuff is often inadequate, leaving patients with persistent symptoms [17]. Because of that, the patient's ability to work and perform daily activities is limited while placing a substantial burden on healthcare systems [1].

Several robots and exoskeletons exist for the rehabilitation of the upper limb [18], [19]. Robotic devices can provide high-intensity, repetitive exercises and target specific injuries/joints. Additionally, the robot can act as a sensor, provide force feedback, and measure joint positions, velocities, accelerations, and torques [20]. These metrics can be monitored objectively and reliably throughout a rehabilitation program to assess the patient's progress [16].

In the case of rehabilitation of rotator cuff tears, monitoring the subject's muscle function is of interest to prevent (re-)tearing of the tendons. The deep-tissue nature of the rotator cuff muscles, combined with the complexity of the glenohumeral (GH) joint, makes it difficult to use lab-based motion-capture and electromyography (EMG) data to measure muscle function of the rotator cuff muscles. Musculoskeletal modeling, in combination with robotic measurements, could provide a physiotherapist with quantitative information on the biomechanics of the shoulder and rotator cuff complex.

A popular open-source software for the development and analysis of musculoskeletal models is OpenSim [21], [22]. A model can account for patient-specific parameters

[1]Department of BioMechanical Engineering and [2]Department of Cognitive Robotics, Delft University of Technology, Delft, The Netherlands

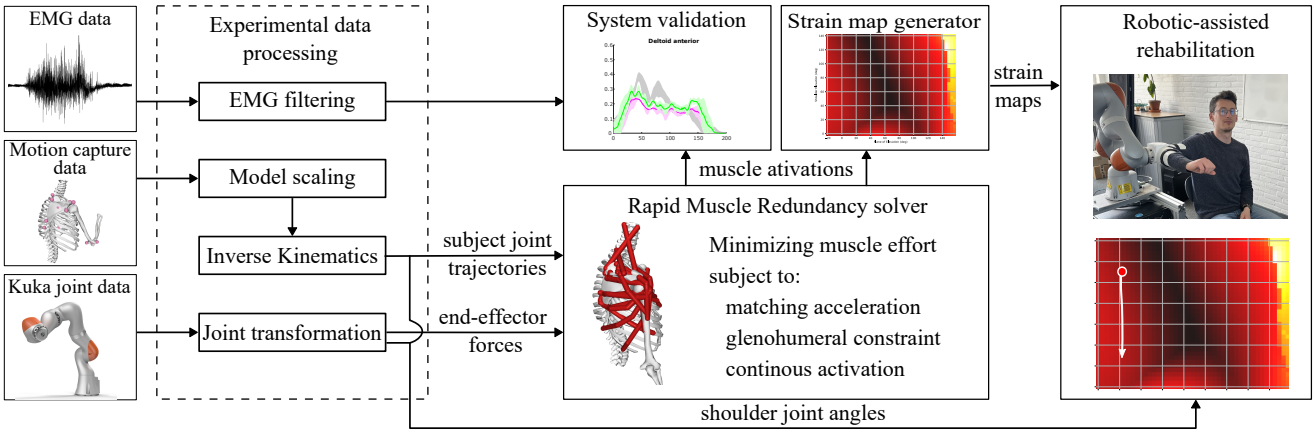

Fig. 1: An overview of the workflow for active robotic-assisted rehabilitation, with quantitative insights into the risk of re-injury. The experimental data is obtained via motion capture using optical markers or shoulder joint estimates during a human-robot interaction. The experimental data is processed to obtain the joint trajectories and external forces. The Rapid Muscle Redundancy solver is used to find the optimal combination of muscle activations for a given trajectory. The estimated muscle activations are validated against experimental EMG data and used to obtain the rotator cuff tendon strains. These strains are visualized in "strain maps" and are used to visualize the internal biomechanics of the shoulder during rehabilitation.

and provide insight into the biomechanics of the human body, such as muscle function, joint reaction forces, and muscle-tendon lengths/strains [23]. Interpretation of the numerous variables the model provides can be difficult for the user, especially if the user has limited experience with the model, such as a physiotherapist, other healthcare professionals, or the patient. It is, therefore, necessary to present this information in an intuitive and meaningful manner. A metric derived from the musculoskeletal model to assess the risk of tearing or re-injury of the rotator cuff muscles is tendon strain.

In our previous work, we showed a way to capture the relationship between the tendon strains and shoulder state in the form of “strain maps” [24] and how to use a collaborative robot to navigate those maps in real-time [25]. These strain maps are an intuitive representation of the rotator cuff tendon strains and can be used to minimize the risk of re-injury of the rotator cuff tendons while maximizing the range of motion. The incorporation of a robot in this rehabilitation process enabled real-time feedback through the segmentation of safe and unsafe strains. Nevertheless, these studies are limited to passive motions by not accounting for the influence of external forces and muscle activations on the muscle-tendon strains.

To address this limitation, this study focuses on the estimation of rotator cuff muscle activations to develop active strain maps for robotic-assisted rehabilitation. Currently, the musculoskeletal modeling software OpenSim offers two methods to estimate muscle activations, namely Static Optimization (SO) [26] and Computed Muscle Control (CMC) [27]. The SO algorithm neglects the passive contribution of muscle fibers and any time-dependent muscle properties, such as the muscle activation dynamics, which leads to gross simplifications in the modeled muscle function [28]. While CMC allows for the integration of the muscle activation dynamics, it comes at a computational cost, making it unsuitable to use in a real-time implementation [29].

When considering modeling of the shoulder joint, an additional layer of complexity arises due to the instability commonly observed in the glenohumeral (GH) joint caused by its great mobility. The larger superficial muscles spanning the GH joint actuate the motion of the joint, with the rotator cuff muscles acting as the main stabilizers of the humerus in the GH fossa. Neither SO nor CMC include a constraint on the joint reaction forces, resulting in possible underestimation of the contribution of stabilizing antagonistic muscles [30].

Several studies acknowledge the importance of considering GH joint stability and include a constraint on the joint reaction forces in the GH joint to account for it [31]–[33]. However, their implementations were not made available. The Rapid Muscle Redundancy (RMR) solver is a newly-developed open-source solver [34]. By (1) including the constraint on the joint reaction force direction in the GH joint, (2) accounting for passive muscle fiber contribution, and (3) activation dynamics, it produces physiologically realistic muscle activation estimations. Leveraging numerical optimization at each time step avoids the computational cost as observed in CMC.

The aim of this study is to expand further on providing a physiotherapist with an accurate and intuitive way to monitor rotator cuff tendon strains during robotic-assisted rehabilitation. To achieve this goal, we leveraged the musculoskeletal model and the RMR solver. These tools allow us to include external forces and muscle activations to accurately estimate tendon strains during motion. By including these necessary elements, the active strain maps

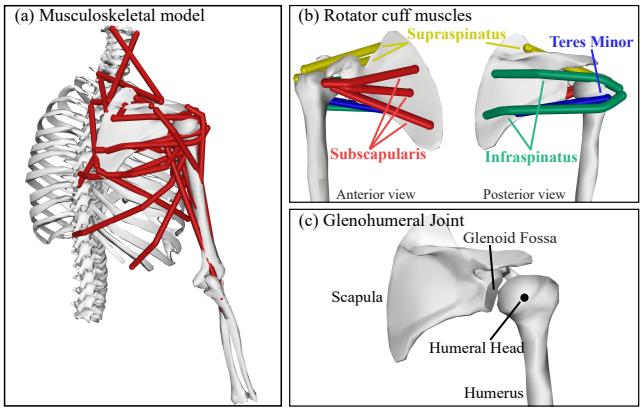

Fig. 2: An overview of the thoracoscapular model. (a) The musculoskeletal shoulder model, and in red, all the actuating muscles. (b) The rotator cuff complex, the four rotator cuff muscles are represented by eight muscle elements; Infraspinatus - green, supraspinatus - yellow, subscapularis - red, teres minor - blue. (c) The glenohumeral joint, detailing the relation between the humeral head and the glenoid fossa of the scapula.

will provide a more complete representation of the strains experienced by the patient. We validated the system on an experimental data set, including motion capture and EMG data [35]. Subsequently, the system was demonstrated and evaluated with the Kuka LBR iiwa collaborative robot arm, which serves as the robot physiotherapist and sensor for external forces applied to the arm and estimator of the shoulder state.

II. Methodology

The aims of our study can be divided into four tasks: 1) musculoskeletal modeling of the shoulder to obtain information on the internal biomechanics during rehabilitation. 2) resolving the muscle redundancy problem to estimate accurate muscle activations by considering active muscle dynamics and the GH joint stability. 3) visualizing rotator cuff tendon strains with maps to provide a physiotherapist with feedback on safe ROM. 4) integration of a robotic device to help guide a patient safely through low-strain zones on the maps. The four tasks are summarized in Figure 1 and described in detail in the sections II-A-II-D. The proposed muscle redundancy solver in Python was first validated against experimental EMG data and the corresponding MATLAB implementation of the muscle redundancy solver, as described in II-E. Finally, an experiment was conducted using a collaborative robot arm to test the complete proposed approach, combining the four tasks needed to achieve the aim of this study (II-F).

A. Musculoskeletal shoulder model

We leveraged the multi-body thoracoscapular model [36] and the open-source modeling tool OpenSim to estimate how the rotator cuff muscles are affected during shoulder rehabilitation [37]. This model is designed to provide high fidelity and accurate representation of the shoulder complex. The movement of the humerus was decoupled from the scapula, allowing for precise modeling of the shoulder motion. The shoulder complex includes a total of four joints describing the complete shoulder kinematics; the thoracoscapular, glenohumeral (GH), acromioclavicular, and sternoclavicular joints. The thoracoscapular joint has four degrees of freedom (DoFs) and utilizes an elliptic surface to represent the thorax the scapula can glide on. The glenohumeral joint is represented as a three degrees-of-freedom (DoFs) gimbal joint. Both the acromioclavicular and sternoclavicular joints are represented as spherical joints [38]. The acromioclavicular and sternoclavicular joints are coupled with the scapula, reducing the DoFs of the shoulder kinematics to seven. The model is actuated by 33 muscle elements, including eight elements representing the four rotator cuff muscles - infraspinatus, subscapularis, supraspinatus, and teres minor. The musculoskeletal model, rotator cuff complex, and glenohumeral joint are shown in Figure 2. Even if the model is carefully constructed, the muscles cannot always generate enough force to match the motion from experimental data due to errors/inaccuracies in the model and/or input data [39]. To account for these inaccuracies, reserve actuators were added to all coordinates individually. This addition is admissible and will still result in a realistic muscle activation estimation as long as the forces produced by the reserve actuators are negligible compared to the muscles.

We added a prescribed force component to the model to represent the interaction forces and torque between the robot and the subject. This force set acts on a fixed location at the elbow and includes two forces and one torque component. The force set is defined in the elbow frame; the forces act along two axes, perpendicular to the humerus (y_{el} and z_{el}), and the torque is along the humeral axis (x_{el}). The magnitude of the force and torque components are updated for every time step. The addition of external forces to the model was tested for a simple and straightforward scenario; the results are presented in Appendix VI-A.

B. Muscle activation estimation

Due to the redundancy in muscle elements (33) compared to the DoFs (7) of the model, a vast amount of solutions for muscle activations that represent a given motion of the system are possible. To cope with this problem, we developed a novel method called RMR solver [34]. This solver accounts for both passive muscle contributions and active muscle dynamics to produce a more physiologically realistic solution. The RMR solver obtains a solution considerably faster than CMC by bypassing the forward integration and instead leverages numerical optimization at each time step, similar to SO. Additionally, we implemented a constraint to account for the GH joint stability in the RMR solver.

The solver only needs joint trajectories and the external forces acting on the subject as input. It has a cost function on the muscle activations a_i for N_m muscles and the controls c_j for N_q reserve actuators to represent the biological

effort. This cost function is a minimization problem on weighted-squared muscle activations and actuator controls for each time step t_k to retrieve the optimal combination of muscle activations $\mathbf{a}_k \in \mathbb{R}^{N_m}$ and reserve actuator controls $\mathbf{c}_k \in \mathbb{R}^{N_q}$:

$$J(\mathbf{a}_k, \mathbf{c}_k) = \sum_{i=1}^{N_m} w_i a_{i,k}^2 + \sum_{j=1}^{N_q} v_j c_{j,k}^2 \ . \tag{1}$$

The weights of the muscle activation w_i and actuator controls v_j are set to 1 and 10, respectively, to promote the engagement of the muscles over the reserve actuators.

The minimization problem was subjected to three additional constraints to ensure a physiologically realistic solution. The first constraint was to ensure that the simulated accelerations matched the experimental ones:

$$\mathbf{A}_{\text{acc},k} \begin{bmatrix} \mathbf{a}_k \\ \mathbf{c}_k \end{bmatrix} = \tilde{\ddot{\mathbf{q}}}_k \ . \tag{2}$$

Here, $\tilde{\ddot{\mathbf{q}}}_k \in \mathbb{R}^{N_q}$ are the subject's joint accelerations due to the active muscle contribution. $\tilde{\ddot{\mathbf{q}}}_k$ is obtained by removing the influences of gravity and passive muscle forces on the recorded experimental joint accelerations of the subject. Element $A_{\text{acc},k}(j,i)$ of $\mathbf{A}_{\text{acc},k} \in \mathbb{R}^{N_q \times (N_m + N_q)}$ represents the influence of a single activation/control of actuator i on the acceleration of coordinate j.

The second constraint was on the joint reaction forces in the glenohumeral joint. This direction of the joint reaction forces was constrained to be within the glenoid fossa to ensure the stability of the GH joint. The shape of the glenoid fossa was considered circular, resulting in the following constraint definition:

$$\left(\frac{\theta_k(\mathbf{a}_k, \mathbf{c}_k)}{\theta_{\max}} \right)^2 - 1 \leq 0 \ , \tag{3}$$

where $\theta_{\max} \in \mathbb{R}$ represents the maximum allowable angle between the joint reaction force and the glenoid center line and is set to 20°, based on cadaver studies [40]. θ_k is the angle between the joint reaction force and glenoid center line based on the optimization values for muscle activations $\mathbf{a}_k$ and actuator controls $\mathbf{c}_k$. The last set of constraints was put on the muscle activation bounds to account for the physiological activation and deactivation rates. A muscle's force generation and relaxation are dependent on the calcium ion concentrations. The model's muscle activation can range between dimensionless 0 and 1. A value of 0 indicates that no calcium is released by the muscle fibers due to depolarization, resulting in no contraction of the fiber and no active force produced. A value of 1 represents a maximum release of calcium and, thus, maximum muscle contraction and force generation. The muscle activation dynamics as defined in OpenSim [41] can be integrated for consecutive time-steps t_k and t_{k-1} to enforce the muscle activation dynamics implicitly for each muscle i:

$$l_{i,k}(a_{i,k-1}) \leq a_{i,k} \leq u_{i,k}(a_{i,k-1}), \tag{4}$$

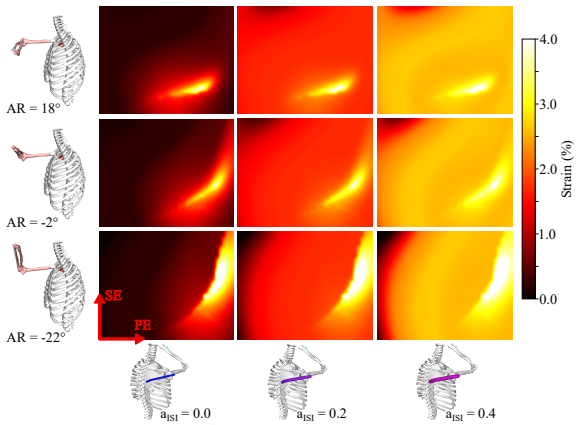

Fig. 3: An overview of how the tendon strain is visualized with strain maps. This example considers the infraspinatus inferior; it includes nine strain maps for a combination of three different axial rotations and three muscle activation levels. The individual maps include the plane of elevation and shoulder elevation on the x- and y-axis, respectively. The columns represent the strain maps for increasing muscle activation of the infraspinatus inferior (a = 0.0, a = 0.2, and a = 0.4). The rows show strain maps for selected axial rotation angles (AR = -22°, AR = -2°, and AR = 18°).

with the lower bound $l_{i,k}$ and upper bound $u_{i,k}$ defined as:

$$l_{i,k}(a_{i,k-1}) = a_{i,k-1} - a_{i,k-1} \left(\frac{1}{2} + \frac{3}{2} a_{k-1} \right) \frac{t_k - t_{k-1}}{\tau_{\text{deact}}}, \text{ and} \tag{5}$$

$$u_{i,k}(a_{i,k-1}) = a_{i,k-i} + \frac{1 - a_{i,k-1}}{\frac{1}{2} + \frac{3}{2} a_{k-1}} \frac{t_k - t_{k-1}}{\tau_{\text{act}}} \ . \tag{6}$$

τ_{act} and τ_{deact} are the activation and deactivation constants and were set to 10 ms and 40 ms, respectively [41]. The lower ($l_{i,k}$) and upper ($u_{i,k}$) bounds were clipped if necessary to ensure that $a_{i,k}$ always falls within the range of [0, 1]. The RMR solver is able to find realistic solutions on par with the currently widely-used solvers CMC and SO. As a result of the implementation of the GH joint constraint, the minimization problem became non-linear. Consequently, the RMR solver employed the numerical solver approach known as Sequential Quadratic Programming (SQP) in MATLAB. A more detailed description of the RMR solver algorithm and its validation against EMG data and the CMC solver is further outlined in [34]. To facilitate the integration of the RMR solver with a robotic device, the solver was re-implemented in Python using the Sequential Least Squares Programming (SLSQP) method. The SLSQP's options do not explicitly set a tolerance on the constraint functions. To account for any numerical errors on the linear equality constraint on the accelerations, a relative tolerance of $\pm 0.1\%$ was added to $\tilde{\ddot{\mathbf{q}}}_k$ in the acceleration constraint. The equality constraint as defined in Equation 2 was converted to a two-sided inequality constraint.

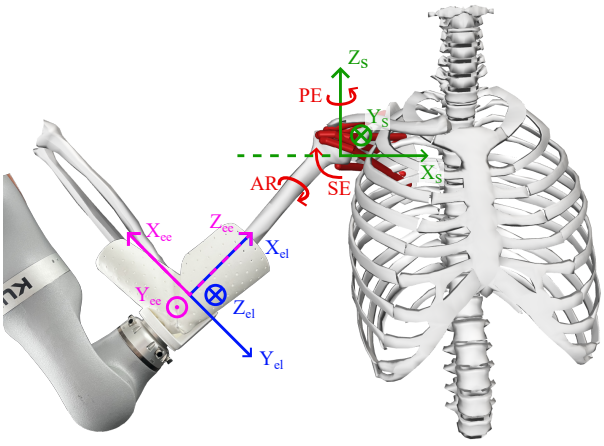

Fig. 4: An overview of the coordinate systems of the setup: The shoulder frame has its origin in the center of the glenohumeral joint (green). The glenohumeral joint DoFs (PE, SE, and AR) are shown in red. The elbow frame (blue) has an origin in the center of the elbow. The elbow frame origin coincides with that of the robot's end-effector frame (pink).

$$\mathbf{l}_k \leq \mathbf{A}_{\text{acc},k} \begin{bmatrix} \mathbf{a}_k \\ \mathbf{c}_k \end{bmatrix} \leq \mathbf{u}_k \ . \tag{7}$$

Values for δ were tested and are described in Appendix VI-C.

C. Strain maps

For the rehabilitation of rotator cuff tears, we use muscle-tendon strains (ε) as a metric to indicate if a shoulder state induces the risk of (re-)tearing the tendon and is defined as:

$$\varepsilon = \frac{l^T - l^0}{l^0} \cdot 100\% \ , \tag{8}$$

with l^T and l^0 the tendon length and tendon slack length, respectively. The tendon strains are calculated for each muscle element separately. These strains can be calculated for any shoulder state and muscle activation combination. The influence of muscle activation on tendon strains is described in Appendix VI-B. The strain estimations need to be combined into a simple, intuitive visualization to be used by a physiotherapist during rehabilitation. The "strain map" is a means to achieve this. The maps give the user a high-resolution visualization of the tendon strain in the joint space. Different modalities can be chosen depending on the patient's injury and progress during therapy. E.g., the strain maps of all rotator cuff muscle elements can be combined into a single strain map by taking the maximum strain for each pose. The strain maps can also represent a single muscle (element) to ensure safe strains for rehabilitation of a specific muscle-tendon unit due to an existing injury.

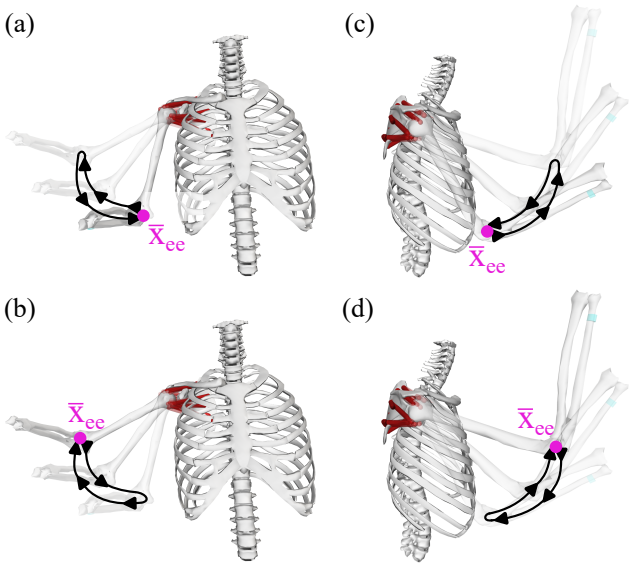

Fig. 5: The four motions as performed during the experiment with (a) abduction, (b) adduction. (c) forward flexion, (d) extension. The start position of each motion was set as the reference pose for the robot $\bar{x}_{\text{ee}}$ (pink), and the subject made one continuous motion as indicated in black. The arrows indicate the direction of the motion.

Since the rotator cuff muscles only span the GH joint, we only consider the three shoulder DoFs α, consisting of the following Euler angles; plane of elevation (PE), shoulder elevation (SE), and axial rotation (AR):

$$\alpha = [\,\text{PE},\ \text{SE},\ \text{AR}\,] \ . \tag{9}$$

The range of shoulder DoFs was constrained within the limits of $-20° \leq PE \leq 160°$, $0° \leq SE \leq 144°$, and $-90° \leq AR \leq 100°$. Rotator cuff tendon strain estimations were calculated for each combination of α at four-degree intervals and muscle activation in 0.005 activation level intervals. The strains were pre-computed to reduce the computational load during rehabilitation.

To visualize the four-dimensional space for a physiotherapist, the strain maps were divided into two-dimensional layers/maps with the plane of elevation and shoulder elevation on the x- and y-axis, respectively. The axial rotation and muscle activation are fixed for every two-dimensional map. A new map is considered by changing either one, as shown in Figure 3.

D. Robotic control and interaction

The strain maps need input about the shoulder state variables and any external forces acting on the patient at any time step to visualize the internal biomechanics of the shoulder joint. A tool that can be used to achieve this is a robotic device. We leveraged the KUKA LBR iiwa, an industrial collaborative robot for physical human-robot interaction with 7 DoFs. The robot is controlled with a Cartesian impedance controller:

Task	Trapezius middle	Trapezius superior	Trapezius inferior	Deltoid anterior	Deltoid posterior	Deltoid middle	Pec.Maj. clavicle	Serratus anterior	Infra-spinatus	Latiss. dorsi	Teres major	Method
Abduction	0.09	**0.11**	0.06	0.09	0.07	0.07	0.02	0.07	0.08	0.06	0.06	MATLAB
	0.09	**0.11**	0.06	0.10	0.06	0.08	0.02	0.06	0.07	0.06	0.05	Python
Abduction +	0.07	**0.11**	0.05	0.07	0.10	0.04	0.03	0.06	0.05	**0.13**	0.08	MATLAB
	0.08	0.10	0.06	0.09	0.09	0.04	0.03	0.05	0.06	**0.13**	0.07	Python
Flexion	0.06	0.07	0.04	0.05	0.05	0.05	0.02	0.05	0.04	0.10	0.07	MATLAB
	0.06	0.07	0.04	0.05	0.05	0.06	0.02	0.06	0.04	0.10	0.06	Python
Flexion +	0.04	0.08	0.02	0.05	0.07	0.04	0.04	0.06	0.02	**0.16**	**0.11**	MATLAB
	0.04	0.08	0.02	0.05	0.06	0.06	0.03	0.06	0.02	**0.17**	0.10	Python
Shrugging	0.02	0.09	0.01	0.01	0.02	0.02	0.06	0.01	0.08	0.03	**0.17**	MATLAB
	0.02	0.09	0.01	0.01	0.01	0.01	0.06	0.01	0.08	0.03	**0.15**	Python
Shrugging +	0.04	0.06	0.02	0.01	0.02	0.02	0.05	0.02	0.02	0.10	**0.12**	MATLAB
	0.04	0.06	0.02	0.01	0.02	0.01	0.05	0.02	0.01	0.10	**0.13**	Python

TABLE I: Mean Absolute Error (MAE) for MATLAB and Python estimates of the muscle activations against the EMG-based activations. MAE values ≥ 0.1 are highlighted. For the comparison of the serratus anterior, both the MATLAB and Python estimations are an average of the three bundles that represent the muscle in the model, as reported in [35].

$$\mathbf{F}_{\text{imp}} = \mathbf{K}(\bar{\mathbf{x}}_{\text{ee}} - \mathbf{x}_{\text{ee}}) + \mathbf{D}(\dot{\bar{\mathbf{x}}}_{\text{ee}} - \dot{\mathbf{x}}_{\text{ee}}) \ . \tag{10}$$

Here, $\mathbf{F}_{\text{imp}} \in \mathbb{R}^6$ is the interaction forces and torques at the end-effector/elbow. The robot's end-effector reference and actual pose are $\bar{\mathbf{x}}_{\text{ee}}$ and $\mathbf{x}_{\text{ee}}$, respectively. $\mathbf{K}$, $\mathbf{D} \in \mathbb{R}^{6\times 6}$ are the desired stiffness and damping matrices in Cartesian space. The positional and rotational stiffness of $\mathbf{K}$ are prescribed, and $\mathbf{D}$ is obtained using the double diagonalization design method [42]. The increase in impedance with distance from the reference pose is used to mimic the effect of elastic bands during rehabilitation exercises.

A custom L-shaped brace is mounted on the robot's end-effector and worn around the elbow of the patient; see Figure 4. This brace allows the robot to know the position in space of the elbow and, subsequently, the shoulder state angles. The robot joint torques are used to estimate the force at the end-effector of the robot, which is acting on the patient's elbow. The joint angles of the robot are used to estimate the three shoulder DoFs and their derivatives. Data from the torque sensors and the joint angles are collected at 200Hz. This data is subsequently used as input for the RMR solver for the muscle activation and tendon strain estimations.

E. System validation

Before we can integrate the muscle activations in the robotic-assisted rehabilitation of the rotator cuff, we need to validate the accuracy of the RMR solver in Python. The results from the Python implementation were compared to filtered experimental EMG data and the results of the RMR solver in MATLAB. The dataset used for validation is openly accessible from a previous study [35]. The set consists of a total of 18 experimental trials. The same subject executed three repetitions of forward flexion, abduction, and shrugging. The three motions were both executed unloaded and with a two-kilogram weight in the hand. For every trial marker data was recorded, capturing the motion of several bony landmarks. Additionally, surface EMG electrodes were used to record eleven muscles.

The motion capture marker data was processed with an updated inverse kinematics analysis to retrieve joint angles from the experimental trajectories. Inverse kinematics tracking weights were applied to the scapula coordinates to maintain a realistic relationship between the scapula upward rotation and shoulder elevation. Subsequently, the obtained joint angles were smoothed using a 4th-order low-pass Butterworth filter with a cut-off frequency of 3 Hz. This filtering step aimed to mitigate any high-frequency noise present in the marker data. The complete dataset was evaluated by comparing the mean absolute error (MAE) between the EMG-recorded muscle activations and the MATLAB and Python solver estimations.

F. Experimental setup

One healthy individual was considered as a subject for the following experiments. The subject was seated in a normal chair, and after the robot was moved to its initial position, the custom arm brace was put on. The subject performed four different movements based on common rehabilitation exercises; forward flexion, extension, abduction, and adduction (see Figure 5). The subject was free to move in space but was instructed to make 1-DoF movements. For forward flexion and extension, the subject was instructed to keep axial rotation and plane of elevation around $-90°$ and $90°$, respectively. In the case of abduction and adduction, axial rotation and plane of elevation were kept around $0°$. To ensure the subject's comfort and safety, the subject was given instructions to restrict their movement within a certain ROM. Therefore, for all cases, shoulder elevation was instructed to be limited between $30°$ and $80°$.

The Cartesian impedance controller of the robot was leveraged to mimic elastic bands commonly used in rehabilitation exercises. By increasing the positional stiffness, a larger external force acted on the elbow; thus, more effort was required from the subject to move along the trajectory. The four movements were all executed for three different positional stiffness values: $K_{pos} = 10$, 30, and 50 N/m. The rotational stiffness was kept constant throughout the experiments. The stiffness value K_{rot} was set to 50

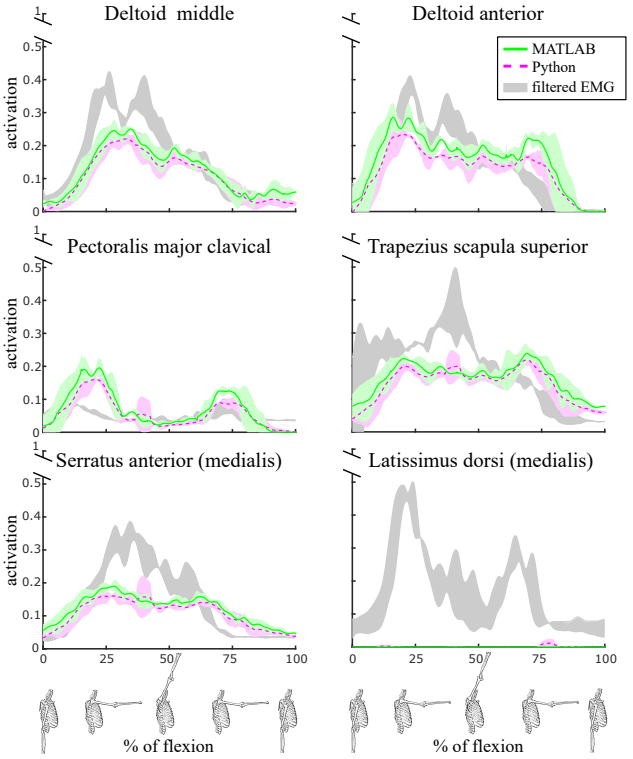

Fig. 6: Muscle activation of selected muscles during a loaded flexion motion. The estimations are shown for MATLAB (green) and Python (pink) and are displayed as the mean over three repetitions of the motion (bold lines), with a shaded ± 1 SD. Additionally, the muscle activations from filtered experimental EMG data are displayed in gray (± 1 SD).

Nm/rad, which is the upper limit before the robot becomes unstable and restricts motion in AR.

To allow for the estimation of shoulder joint angles based on the robot joint angles, the subject was instructed not to move his torso. The shoulder frame was therefore assumed to be fixed relative to the robot. Thus a constant transformation between the robot end-effector frame and the shoulder frame was possible. During the experiments with the robot, we only obtained information on the GH joint coordinates and thus assumed that the scapula was not moving during the muscle activation estimation. The shoulder state and external force data were post-processed to estimate the muscle activations and the tendon strains and generate the strain maps.

All the computations were run on an HP ZBook Studio G3 running Windows 10 with an Intel i7-6700HQ processor and 8GB RAM. The RMR solver was coded in MATLAB R2022a and Python 3.8. The experimental dataset used for validation provided input at 100 Hz, whereas the robotic control loop and data stream ran at 200 Hz.

III. Results

In this section, we present our results beginning with the comparison between the MATLAB and Python solver results as a validation of the Python solver. The estimated muscle activations from both solvers were compared to experimental EMG data as a benchmark. We also computed the computational cost of the solver (III-A). Next, we show the resulting muscle activations and tendon strains from the conducted experiments with a robotic device for a set of motions and show the effect of external forces on the muscle activations and, subsequently, the tendon strains (III-B). Finally, we show the resulting strain maps, which now represent active model-based tendon strain estimations during human-robot interaction in III-C.

	Abduction	Flexion	Shrugging	Average
Unloaded	5.5	4.8	5.3	5.2
Loaded	5.7	4.3	4.3	4.7
Average	5.6	4.5	4.8	5.0

TABLE II: Frequency of the RMR solver in Python over a dataset consisting of 18 trials collected at 100 Hz. They are summarized per motion and loading conditions. Overall, the RMR solver implemented in Python runs at an average of 5 frames per second.

A. Validation of Python RMR solver

Muscle activations estimated with the RMR solver in MATLAB and Python were compared to the experimental EMG data. The activation was averaged over the three repetitions for each task. The muscle activation estimations were compared during three motions; abduction, flexion, and shrugging for the unloaded and 2 kg load condition. To capture differences across the dataset, mean absolute errors (MAE) were computed and are summarized in Table I. The MAE values for MATLAB and Python against EMG-based activations are ≤ 0.17, with most values ≤ 0.10. For the majority of the activation estimations, the errors against EMG data are the same in the MATLAB and Python implementations. The differences in MAE values between MATLAB and Python are ≤ 0.02. Figure 6. The figure includes the mean and standard deviation of muscle activations for selected muscles during a loaded flexion task. The results from the experimental EMG data and the MATLAB and Python implementation are shown.

We ran the RMR solver in Python for all (18) trials to get an average frequency at which the solver can run. The frequencies are summarized in Table II. The resulting frequencies are presented for the three motions in unloaded and loaded conditions. The frequency at which the solver runs varies between 4.3 Hz and 5.7 Hz, with an overall average of 5 Hz, which is the same frequency as the MATLAB implementation [34].

B. Muscle activation and tendon strain estimation

The resulting muscle activation and tendon strains for the experiments performed with the Kuka LBR iiwa robotic arm are presented below. Two of the motions are shown, each with a different rotator cuff muscle highlighted. Figure 7 shows the resulting muscle activation and tendon strain of

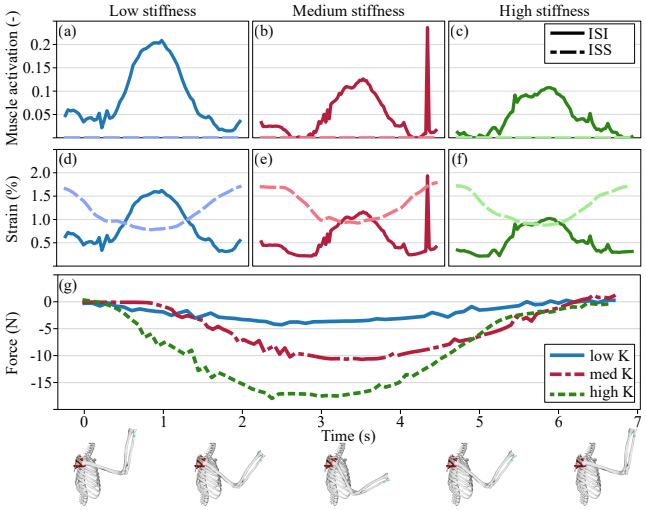

Fig. 7: An example of the shoulder extension movement and the estimated muscle strain and tendon activation of the infraspinatus inferior (ISI) and infraspinatus superior (ISS). The muscle activations (a-c) and tendon strains (d-f) are shown for all three robot stiffness values. In (g), the magnitude of the external force at the elbow is shown for the three different conditions.

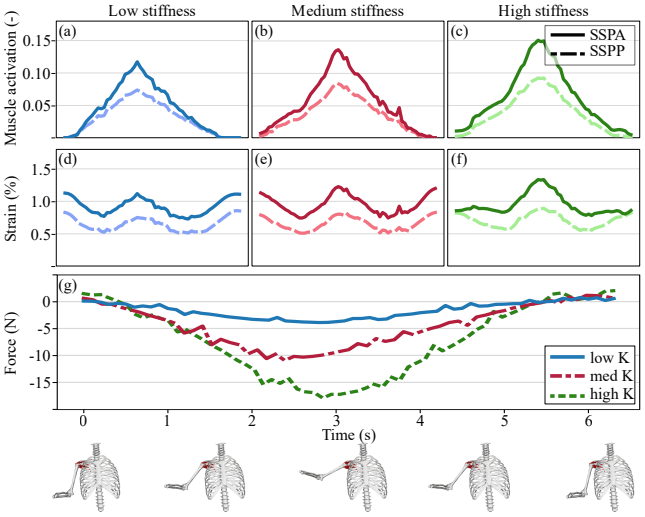

Fig. 8: An example of the shoulder abduction movement and the estimated muscle strain and tendon activation of the supraspinatus anterior (SSPA) and supraspinatus posterior (SSPP). The muscle activations (a-c) and tendon strains (d-f) are shown for all three robot stiffness values. In (g), the magnitude of the external force at the elbow is shown for the three different conditions.

the infraspinatus inferior and infraspinatus superior during extension. A single extension was performed for three different robot stiffness values ($K = 10$ N/m, $K = 30$ N/m, and $K = 50$ N/m). By increasing the stiffness, the magnitude of the external force also increases. During extension, the infraspinatus superior is not activated for any of the modalities. The infraspinatus inferior is recruited less when the stiffness is increased, and the infraspinatus inferior tendon strain also reduces with higher stiffness. A peak at the end of the motion with medium stiffness can be seen in the infraspinatus inferior muscle activation and tendon strain. The supraspinatus muscle bundles are highlighted during a single abduction motion, again for all three stiffness values (Figure 8). Both the supraspinatus anterior and posterior bundles were activated during the abduction task. The estimated muscle activation increased with a higher positional stiffness of the robot, which also resulted in a higher tendon strain.

C. Strain maps during active rotator cuff rehabilitation

Using strain maps, we visualized the tendon strains during a single abduction motion with medium positional robot stiffness. A subset of the resulting strain maps is shown in Figure 9. They represent the strain distribution for five instances in time throughout the motion. An example of strain maps is shown for subscapularis inferior (SSCI), infraspinatus superior (ISS), and the maximum strain of all rotator cuff muscles. These maps exhibit varying shapes as the shoulder pose and muscle activation levels change throughout the motion, resulting in a shift of low and high-strain zones. Notably, the two individual muscle elements experience high strains at different shoulder poses.

IV. Discussion

In this study, we developed a method to gain insight into the inner biomechanics of the shoulder complex during active rehabilitation exercises. We examined and developed a deeper understanding of the recruitment of the rotator cuff muscles during various motions and loading conditions. With this new information, we present a framework to provide a physiotherapist with an intuitive interpretation of the data to allow for safe rehabilitation of the rotator cuff muscles based on quantitative tendon strains. The strain maps and better understanding of the rotator cuff functions enable further exploration, development, and, ultimately, improvement of robotic-assisted rehabilitation of the rotator cuff muscles.

The RMR solver in Python has a similar computational cost as it had in MATLAB and can solve at 5 Hz. Considering that the frequency of human movement typically falls within the range of 0 to 10 Hz [43] and will likely be slower during rehabilitation, our solver's efficient computational time allows for real-time estimation of muscle activation. More notably, this method offers a distinguished advantage over the previous solver as it enables real-time consideration of external forces. This is a significant step forward in biomechanics-aware rehabilitation of the shoulder.

To showcase the proposed framework, we conducted several experiments using the Kuka LBR iiwa robotic arm as a proof-of-concept for robotic rehabilitation. The impedance controller of the robot was used to mimic the use of elastic bands during therapy. The developed solver serves as a powerful tool to reveal information regarding the activation

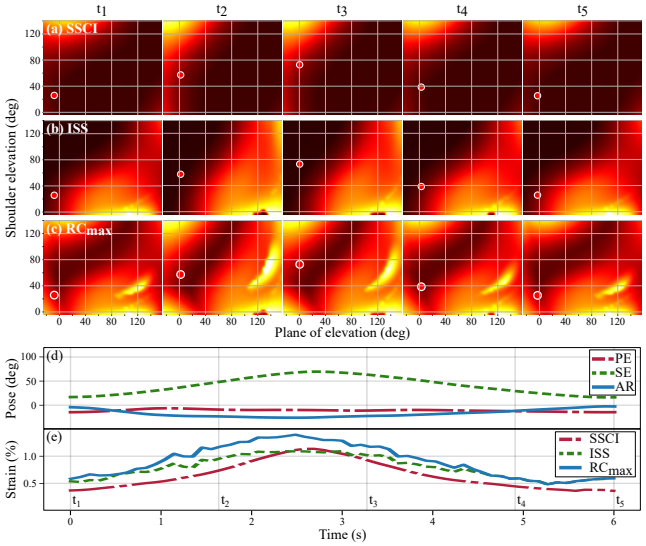

Fig. 9: An example of strain maps visualizing tendon strain at five instances ($t_1 - t_5$) during a single abduction motion with a medium stiffness (K=30 N/m). The strain maps are shown for the a) subscapularis inferior (SSCI), b) infraspinatus superior (ISS), and c) the maximum strain of all rotator cuff muscles. For the complete movement, (d) the shoulder pose and e) selected rotator cuff tendon strains are shown.

levels and recruitment of the rotator cuff muscles during rehabilitation exercises. In the exemplary shoulder extension experiment, we observed an increased engagement of the infraspinatus inferior as a response to the larger external forces applied to the subject (Figure 7. Notably, the tendon strains are also subjected to changes in shoulder pose, as observed in the infraspinatus superior. An opposing muscle response to external forces was observed in Figure 8, where the supraspinatus superior and supraspinatus inferior were activated less for higher forces.

The rotator cuff muscles are the main stabilizers of the glenohumeral joint but also assist in the motions of the shoulder joint. The recruitment of the supraspinatus during abduction aligns with our intuition around shoulder biomechanics for the different external forces. The supraspinatus assists the deltoids in abduction; bigger recruitment of both muscles was observed for increased antagonistic external forces. The infraspinatus is known as the main external rotator of the humeral head, so engagement during the extension motion, with a 90° external rotation of the humerus, is in line with the expectations. We expected larger external forces to destabilize the glenohumeral joint and, thus, a higher engagement of the rotator cuff muscles, which was not the case for the infraspinatus inferior during extension. This may be explained by an observed increase in latissimus dorsi muscle activation, which helps depress the humerus inside the glenohumeral joint, and requires less stabilizing efforts from the infraspinatus.

It is important to gain insight into the rotator cuff muscle recruitment patterns to understand how a patient should or should not move during rehabilitation to prevent injury. The musculoskeletal model-based RMR solver is unique in its ability to make these estimates in real-time and offers opportunities to develop new novel rehabilitation exercises tailored to the patient. During the initial phases of rehabilitation, the priority lies in preventing the aggravation of a tear or the occurrence of a re-tear following surgical repair. Using the strain estimates from the solver, a physiotherapist can choose the robot's stiffness so that the strains in the damaged muscles are below a certain threshold. For example, in the case of an injured infraspinatus, a higher stiffness during extension was observed to reduce the strains. Conversely, during the later stages of rehabilitation, a physiotherapist may desire to prioritize strengthening a specific muscle or recruit compensatory muscles to compensate for an injured one. The combination of a customizable robotic device and the solver presents an intriguing opportunity to design and evaluate novel rehabilitation exercises for various rotator cuff disorders. This approach allows for exploring and establishing tailored rehabilitation protocols, providing valuable insights for optimizing patient recovery and improving outcomes.

We visualized the strains in intuitive 2D maps to be used during rehabilitation by a physiotherapist. These maps provide information on the tendon strain in the current shoulder state and the surrounding poses. With the strain maps, we can visualize quantitatively shoulder states that will reduce the risk of re-injury while increasing ROM to improve recovery. The strain maps presented in this study include the effect of external forces and muscle activations on the tendon strains and represent more physiologically realistic strains. This is an important extension of our previous work that was limited to considering only passive strains [24], [25]. The maps offer a physiotherapist an intuitive metric to determine safe and unsafe poses in real-time during rehabilitation. Depending on the patient and the stage in the rehabilitation process, the maps can be customized to show a single muscle, a combination of a few, or all rotator cuff muscles combined.

Several limitations of this study can be identified. The model in our study did not reflect the actual anatomical and physiological parameters of the subject. To improve muscle activation and tendon strain estimations, a subject-specific model could be considered, facilitating personalized rehabilitation strategies.

The muscle activations and tendon strains peak on some rare occasions, as was observed for the infraspinatus inferior during extension. No direct cause could be found that explains this behavior; the muscle length is continuous, and the optimizer converges to a solution. However, the cost value was larger than the adjacent time steps. A similar peak was observed during flexion, where the peak seems to stem from a discontinuity in the fiber length of the subscapularis medialis, which subsequently influences the solver's attempt to find an equilibrium for all muscles (see Appendix VI-D). The peaks seem to have different causes and are infrequent in the limited dataset collected with the robot. More data and further investigations are needed to understand which

mechanisms cause the peaks, such as the muscle's geometry, the definition of the cost function, or the solver's parameters.

We simplified the data collection process using a robotic device. The robot captures data on the estimated external forces and shoulder joint state that can directly be used to estimate muscle activation. However, it comes with certain assumptions. To be able to estimate the shoulder joint state from the robot configuration, we assumed a static shoulder frame and scapula throughout the movement, not capturing the complete kinematics of the shoulder. Tracking the scapula movement can further clarify the engagement of the rotator cuff muscles and ensure safe strains during rehabilitation [44].

Lastly, the inclusion of muscle activation in tendon strain analysis provides a physiologically realistic perspective but introduces additional complexity. Muscle activation estimations, and thus the tendon strains, are influenced by the external forces applied to the subject and the shoulder state. Especially changes in force are unpredictable, making it uncertain how the strain space will evolve in the subsequent time step. For clinical implementation, further investigation is required to enable real-time updates of active strain maps while incorporating the previously identified safe and unsafe strain zones [25].

V. Conclusion

We developed the RMR solver, a novel computational tool that computes realistic muscle activations during motion. It considers the GH joint stability, active muscle dynamics, and passive muscle contributions at a low computational cost. The solver was re-implemented in Python and expanded to include the interaction forces and torque between the robot and the subject during active rotator cuff rehabilitation. The provided framework provides physiotherapists with safe and unsafe ROM during rehabilitation, using quantitative information on tendon strains visualized using strain maps. The strain maps can be generated for every muscle element separately or can be used to represent the maximum strain experienced by the rotator cuff complex. We can mimic the resistance forces from elastic bands by changing the robot's stiffness. Physiotherapists can leverage the different active strain maps and robot control settings to deliver therapy for specific injuries in a large ROM without risking re-injury.

References

[1] K. Walker-Bone, K. T. Palmer, I. Reading, D. Coggon, and C. Cooper, "Prevalence and impact of musculoskeletal disorders of the upper limb in the general population," *Arthritis Rheum.*, vol. 51, no. 4, pp. 642–651, Aug. 2004.

[2] M. Urwin, D. Symmons, T. Allison, T. Brammah, H. Busby, M. Roxby, A. Simmons, and G. Williams, "Estimating the burden of musculoskeletal disorders in the community: The comparative prevalence of symptoms at different anatomical sites, and the relation to social deprivation," *Annals of the Rheumatic Diseases*, vol. 57, no. 11, pp. 649–655, 1998, ISSN: 0003-4967. DOI: 10.1136/ard.57.11.649.

[3] M. Khan and J. J. P. Warner, "Cochrane in CORR ®: Manual therapy and exercise for rotator cuff disease," *Clin. Orthop. Relat. Res.*, vol. 475, no. 7, pp. 1779–1785, Jul. 2017.

[4] B. Mazuquin, M. Moffatt, P. Gill, J. Selfe, J. Rees, S. Drew, and C. Littlewood, "Effectiveness of early versus delayed rehabilitation following rotator cuff repair: Systematic review and meta-analyses," *PLoS One*, vol. 16, no. 5, e0252137, May 2021.

[5] H. Minagawa, N. Yamamoto, H. Abe, M. Fukuda, N. Seki, K. Kikuchi, H. Kijima, and E. Itoi, "Prevalence of symptomatic and asymptomatic rotator cuff tears in the general population: From mass-screening in one village," *J. Orthop.*, vol. 10, no. 1, pp. 8–12, Feb. 2013.

[6] C Milgrom, M Schaffler, S Gilbert, and M van Holsbeeck, "Rotator-cuff changes in asymptomatic adults. the effect of age, hand dominance and gender," *J. Bone Joint Surg. Br.*, vol. 77, no. 2, pp. 296–298, Mar. 1995.

[7] F. Jobe, R. Kvitne, and C. Giangarra, "Shoulder pain in the overhand or throwing athlete. the relationship of anterior instability and rotator cuff impingement," *Orthopaedic review*, vol. 18, no. 9, 963—975, Sep. 1989, ISSN: 0094-6591.

[8] G. K. Singh, S. Srivastava, M. Kumar, and S. Ratnakar, "Effects of selected rehabilitative exercises on external rotator muscles and trapezius muscles of masonry workers," *Work*, vol. 60, no. 3, pp. 437–444, 2018.

[9] S. T. Seroyer, S. J. Nho, B. R. Bach Jr, C. A. Bush-Joseph, G. P. Nicholson, and A. A. Romeo, "Shoulder pain in the overhead throwing athlete," *Sports Health*, vol. 1, no. 2, pp. 108–120, Mar. 2009.

[10] U. G. Longo, A. Berton, L. Risi Ambrogioni, D. Lo Presti, A. Carnevale, V. Candela, G. Stelitano, E. Schena, A. Nazarian, and V. Denaro, "Cost-effectiveness of supervised versus unsupervised rehabilitation for rotator-cuff repair: Systematic review and meta-analysis," *Int. J. Environ. Res. Public Health*, vol. 17, no. 8, p. 2852, Apr. 2020.

[11] C. Littlewood, P. Malliaras, and K. Chance-Larsen, "Therapeutic exercise for rotator cuff tendinopathy: A systematic review of contextual factors and prescription parameters," *Int. J. Rehabil. Res.*, vol. 38, no. 2, pp. 95–106, Jun. 2015.

[12] J Kukkonen, A Joukainen, J Lehtinen, K. T. Mattila, E. K. J. Tuominen, T Kauko, and V Aärimaa,

"Treatment of non-traumatic rotator cuff tears: A randomised controlled trial with one-year clinical results," *Bone Joint J.*, vol. 96-B, no. 1, pp. 75–81, Jan. 2014.

[13] P. C. Lastayo, T Wright, R Jaffe, and J Hartzel, "Continuous passive motion after repair of the rotator cuff. a prospective outcome study," *J. Bone Joint Surg. Am.*, vol. 80, no. 7, pp. 1002–1011, Jul. 1998.

[14] T. Proietti, V. Crocher, A. Roby-Brami, and N. Jarrasse, "Upper-limb robotic exoskeletons for neurorehabilitation: A review on control strategies," *IEEE reviews in biomedical engineering*, vol. 9, pp. 4–14, 2016.

[15] B. Østerås, H. Østerås, T. A. Torstensen, and O. Vasseljen, "Dose-response effects of medical exercise therapy in patients with patellofemoral pain syndrome: A randomised controlled clinical trial," *Physiotherapy*, vol. 99, no. 2, pp. 126–131, Jun. 2013.

[16] G. Prange, M. Jannink, C. Groothuis-Oudshoorn, H. Hermens, and M. IJzerman, "Systematic review of the effect of robot-aided therapy on recovery of the hemiparetic arm after stroke," *Journal of rehabilitation research and development*, vol. 43, pp. 171–84, Mar. 2006. DOI: 10.1682/JRRD.2005.04.0076.

[17] K. Yamaguchi, A. Tetro, O. Blam, B. A. Evanoff, S. A. Teefey, and W. D. Middleton, "Natural history of asymptomatic rotator cuff tears: A longitudinal analysis of asymptomatic tears detected sonographically," *Journal of Shoulder and Elbow Surgery*, vol. 10, no. 3, pp. 199–203, 2001, ISSN: 1058-2746. DOI: https://doi.org/10.1067/mse.2001.113086.

[18] A. S. Niyetkaliyev, S. Hussain, M. H. Ghayesh, and G. Alici, "Review on design and control aspects of robotic shoulder rehabilitation orthoses," *IEEE Transactions on Human-Machine Systems*, vol. 47, no. 6, pp. 1134–1145, 2017.

[19] L. Marchal-Crespo and D. J. Reinkensmeyer, "Review of control strategies for robotic movement training after neurologic injury," *Journal of neuroengineering and rehabilitation*, vol. 6, no. 1, p. 20, 2009.

[20] S. Masiero, A. Celia, G. Rosati, and M. Armani, "Robotic-assisted rehabilitation of the upper limb after acute stroke," *Archives of Physical Medicine and Rehabilitation*, vol. 88, no. 2, pp. 142–149, 2007, ISSN: 0003-9993. DOI: https://doi.org/10.1016/j.apmr.2006.10.032.

[21] S. L. Delp, F. C. Anderson, A. S. Arnold, P. Loan, A. Habib, C. T. John, E. Guendelman, and D. G. Thelen, "Opensim: Open-source software to create and analyze dynamic simulations of movement," *IEEE transactions on biomedical engineering*, vol. 54, no. 11, pp. 1940–1950, 2007.

[22] A. Seth, J. L. Hicks, T. K. Uchida, A. Habib, C. L. Dembia, J. J. Dunne, C. F. Ong, M. S. DeMers, A. Rajagopal, M. Millard, *et al.*, "OpenSim: Simulating musculoskeletal dynamics and neuromuscular control to study human and animal movement," *PLoS computational biology*, vol. 14, no. 7, e1006223, 2018.

[23] S. H. Smith, R. J. Coppack, A. J. van den Bogert, A. N. Bennett, and A. M. Bull, "Review of musculoskeletal modelling in a clinical setting: Current use in rehabilitation design, surgical decision making and healthcare interventions," *Clinical Biomechanics*, vol. 83, p. 105 292, 2021, ISSN: 0268-0033. DOI: https://doi.org/10.1016/j.clinbiomech.2021.105292.

[24] J. M. Prendergast, S. Balvert, T. Driessen, A. Seth, and L. Peternel, "Biomechanics aware collaborative robot system for delivery of safe physical therapy in shoulder rehabilitation," *IEEE Robotics and Automation Letters*, vol. 6, no. 4, pp. 7177–7184, 2021. DOI: 10.1109/LRA.2021.3097375.

[25] S. Balvert, J. M. Prendergast, I. Belli, A. Seth, and L. Peternel, "Enabling patient-and teleoperator-led robotic physiotherapy via strain map segmentation and shared-authority," *2022 IEEE-RAS 21st International Conference on Humanoid Robots (Humanoids)*, IEEE, 2022, pp. 246–253.

[26] J. A. Reinbolt, *Static optimization opensim*, 2012-2023. [Online]. Available: https://github.com/opensim-org/opensim-core/blob/main/OpenSim/Analyses/StaticOptimization.cpp.

[27] D. G. Thelen, "Adjustment of muscle mechanics model parameters to simulate dynamic contractions in older adults," *J. Biomech. Eng.*, vol. 125, no. 1, pp. 70–77, 2003.

[28] F. E. Zajac, "Muscle and tendon: Properties, models, scaling, and application to biomechanics and motor control.," *Critical reviews in biomedical engineering*, vol. 17, no. 4, pp. 359–411, 1989.

[29] Y.-C. Lin, T. Dorn, A. Schache, and M. Pandy, "Comparison of different methods for estimating muscle forces in human movement," *Proceedings of the Institution of Mechanical Engineers. Part H, Journal of engineering in medicine*, vol. 226, pp. 103–12, Feb. 2012. DOI: 10.1177/0954411911429401.

[30] A. Kian, C. Pizzolato, M. Halaki, K. Ginn, D. Lloyd, D. Reed, and D. Ackland, "Static optimization underestimates antagonist muscle activity at the glenohumeral joint: A musculoskeletal modeling study," *Journal of biomechanics*, vol. 97, p. 109 348, 2019.

[31] F. Steenbrink, J. H. de Groot, H. Veeger, F. van der Helm, and P. Rozing, "Glenohumeral stability in simulated rotator cuff tears," *Journal of biomechanics*, vol. 42, no. 11, pp. 1740–1745, 2009.

[32] N. Assila, S. Duprey, and M. Begon, "Glenohumeral joint and muscles functions during a lifting task," *Journal of biomechanics*, vol. 126, p. 110 641, 2021.

[33] D. C. McFarland, A. G. Brynildsen, and K. R. Saul, "Sensitivity of neuromechanical predictions to choice

of glenohumeral stability modeling approach," *Journal of Applied Biomechanics*, vol. 36, no. 4, pp. 249–258, 2020.

[34] I. Belli, S. Joshi, J. M. Prendergast, **I. Beck**, C. Della Santina, L. Peternel, and A. Seth, "Does enforcing glenohumeral joint stability matter? a new rapid muscle redundancy solver highlights the importance of non-superficial shoulder muscles," *PLoS Computational Biology*, submitted.

[35] A. Seth, M. Dong, R. Matias, and S. Delp, "Muscle contributions to upper-extremity movement and work from a musculoskeletal model of the human shoulder," *Frontiers in neurorobotics*, vol. 13, p. 90, 2019.

[36] A. Seth, R. Matias, A. P. Veloso, and S. L. Delp, "A biomechanical model of the scapulothoracic joint to accurately capture scapular kinematics during shoulder movements," *PloS one*, vol. 11, no. 1, e0141028, 2016.

[37] S. L. Delp, F. C. Anderson, A. S. Arnold, P. Loan, A. Habib, C. T. John, E. Guendelman, and D. G. Thelen, "Opensim: Open-source software to create and analyze dynamic simulations of movement," *IEEE transactions on biomedical engineering*, vol. 54, no. 11, pp. 1940–1950, 2007.

[38] F. van der Helm, "A finite element musculoskeletal model of the shoulder mechanism," *Journal of Biomechanics*, vol. 27, no. 5, pp. 551–569, 1994, ISSN: 0021-9290. DOI: https://doi.org/10.1016/0021-9290(94)90065-5.

[39] J. L. Hicks, T. K. Uchida, A. Seth, A. Rajagopal, and S. L. Delp, "Is my model good enough? best practices for verification and validation of musculoskeletal models and simulations of movement," *Journal of biomechanical engineering*, vol. 137, no. 2, 2015.

[40] S. Lippitt and F. Matsen, "Mechanisms of glenohumeral joint stability.," *Clinical orthopaedics and related research*, no. 291, pp. 20–28, 1993.

[41] [Online]. Available: https://simtk-confluence.stanford.edu:8443/display/OpenSim/First-Order+Activation+Dynamics.

[42] A. Albu-Schaffer, C. Ott, U. Frese, and G. Hirzinger, "Cartesian impedance control of redundant robots: Recent results with the DLR-light-weight-arms," *2003 IEEE International Conference on Robotics and Automation*, vol. 3, 2003, pp. 3704–3709.

[43] D. A. Winter, *Biomechanics and motor control of human movement*, 4th ed. Chichester, England: John Wiley & Sons, Sep. 2009.

[44] D. C. Teixeira, L. Alves, and M. Gutierres, "The role of scapular dyskinesis on rotator cuff tears: A narrative review of the current knowledge," *EFORT Open Rev.*, vol. 6, no. 10, pp. 932–940, Oct. 2021.

VI. Appendix

A. Validation of external forces

The expansion of the RMR solver with external forces was validated first in a static pose using the thoracoscapular model. The shoulder DoF α was set to $[0, 90, 60]$ degrees. The external force was applied at the elbow in the positive global Y-direction (see Figure 10b). To test the response of the Rapid Muscle Redundancy solver, the force was simulated as a step function:

$$F_y(t) = \begin{cases} 0, & \text{if } t \leq 0.2. \\ 20, & \text{if } 0.2 < t \leq 0.4. \\ 50, & \text{if } 0.4 < t \leq 0.6. \\ 100, & \text{if } 0.6 < t \leq 0.8. \\ 200, & \text{if } t > 0.8. \end{cases}$$

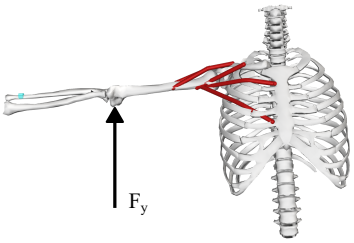

Fig. 10: The external force applied at the elbow in positive Y (global). The deltoid and pectoralis major muscles are highlighted.

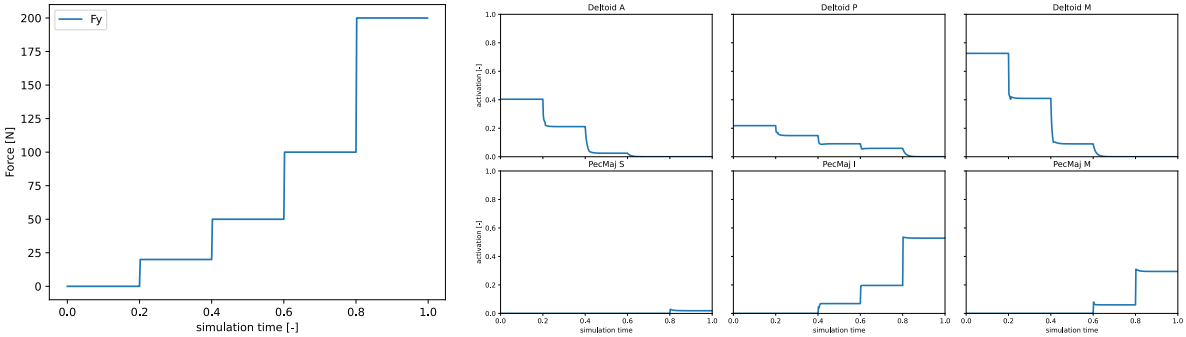

Fig. 11: The external force step function and the response of selected muscles; deltoids and pectoralis majors.

We illustrate the computed muscle activations for the deltoid anterior, medialis, and posterior, along with the pectoralis major superior, medialis, and inferior. The deltoid muscles play a significant role in abduction, while the pectoralis major muscles primarily contribute to adduction. As the force magnitude increases, it was anticipated that the deltoid muscles would be less engaged while the pectoralis major muscles would become more involved. This observation is evident in Figure Figure 11, confirming the successful integration of external forces into our implementation. We can also see the effect of the constraint on the muscle activation bounds on the muscle activations every time the force magnitude changes. Due to the activation and deactivation rates, the muscle activations do not convert instantaneously. This can especially be observed in the deactivating deltoid muscles, since $t_{\text{deact}} > t_{\text{act}}$.

B. *Muscle activation influence on strain estimation*

We verified the influence of muscle activations on tendon strains using the dataset presented in [35]. The comparison between strains with(out) muscle activations is presented in Figure 12. Figure 12a shows the muscle activations and strains for the supraspinatus inferior and superior during an abduction, and Figure 12b shows the three subscapularis muscle elements during flexion. We can see in both cases that even a relatively small muscle activation of 0.1 influences the strain estimation. It is therefore important to also consider muscle activations in the strain map visualization to ensure a safe rehabilitation process.

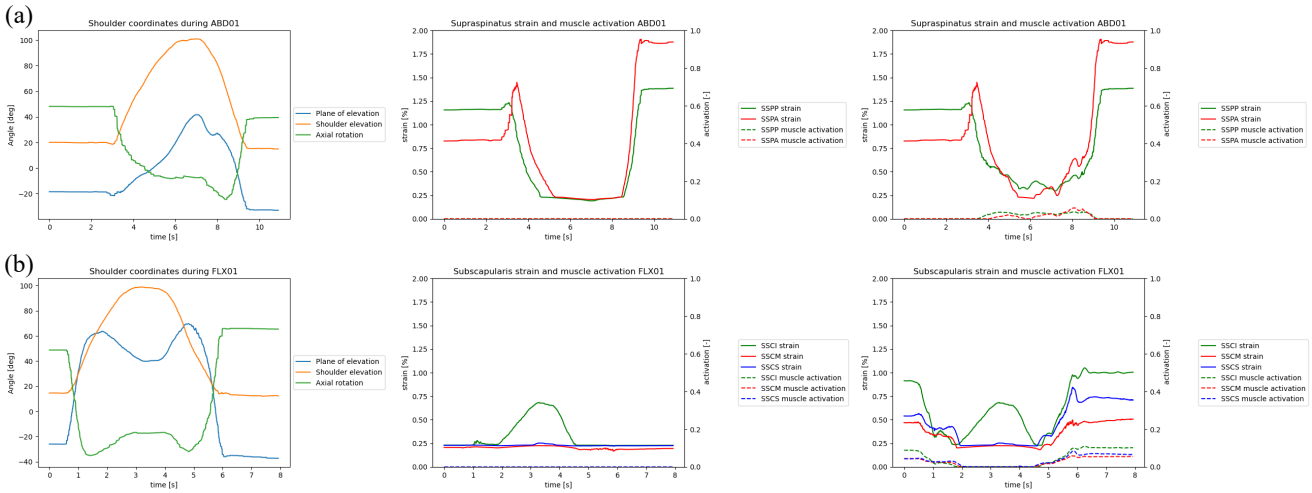

Fig. 12: Examples of the influence of muscle activation on tendon strain estimations, with the left column the shoulder coordinates, the middle column the strain estimations without muscle activations, and the right column the strain estimations with muscle activations for (a) abduction and the supraspinatus superior and inferior muscles and (b) flexion and the subscapularis inferior, medialis, and superior muscle elements.

C. Appendix C: Solver optimization settings

Although carefully considered, the solver in Python has slightly different functionalities to the MATLAB solver. We tested different parameters, trying to balance computational cost and finding a good solution. The findings are presented in the explanatory Figure 13, which showcases the deltoid medialis during an abduction task from the dataset presented in [35].

One of the changes we made was changing the equality constraint (Equation 2) to a two-sided inequality constraint. The added tolerance was kept as low as possible to keep the solution space small. We choose a δ of 0.001, with larger values for δ diverging from the MATLAB solution as shown in the left figure in Figure 13.

We also tested some of the different values of ftol (right figure), which defines the tolerance on the overall cost function. Again they were compared to the MATLAB solution. For the deltoid muscle, we do not observe any notable differences between any of the values for ftol. We opted to use ftol $= 1e^{-06}$ in the end.

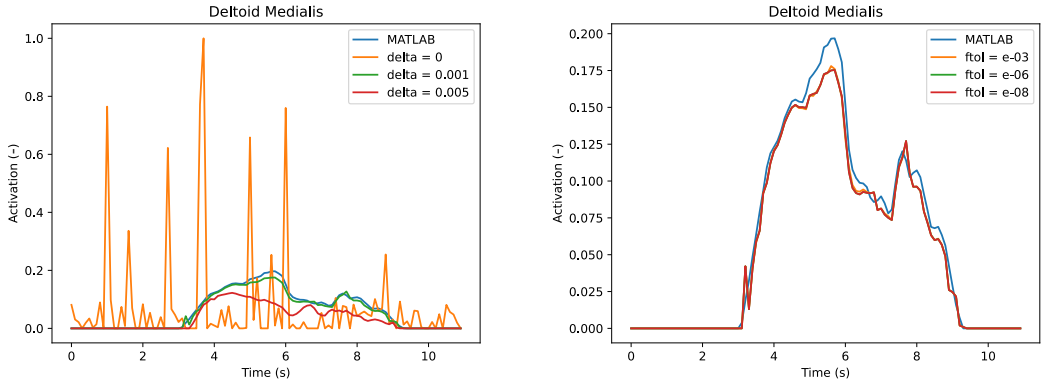

Fig. 13: Comparison of the deltoid medialis activation during abduction

D. *Investigating peaks in muscle activation and strains*

During some of the experiments, the muscle activation and/or tendon strain show a discontinuity in the form of peaks. We need to understand and act accordingly on these discontinuities to be able to use the framework in a clinical setting, such as rehabilitation. We believe that some of the peaks might be explained by the wrapping paths used to define the shape of the muscle elements in the thoracoscapular muscle. Figure 14a shows an incidence of such peak during flexion with $K_{\text{pos}} = 50$ N/m. It includes the muscle activations and strains of the teres minor and subscapularis muscles. We investigated the lengths of all muscle elements during the motion and observed that the subscapularis medialis length had a peak at the same time as the activation and strain peak (Figure 14b). Although this behavior of the muscle raises questions regarding the model's wrapping methods, it is only observed sporadically and is not always found to be the cause of the peaks. We could not find a discontinuity in a muscle's geometry that might explain the peak we observed in Figure 7. Thus further investigation is required to identify the underlying mechanisms of the different peak occurrences.

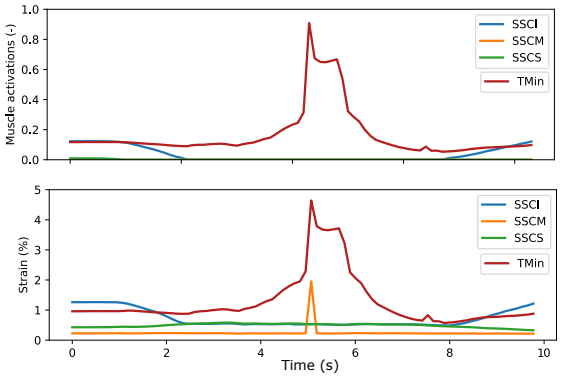

(a) Muscle activation and tendon strains for the subscapularis inferior, medialis, superior and the teres minor

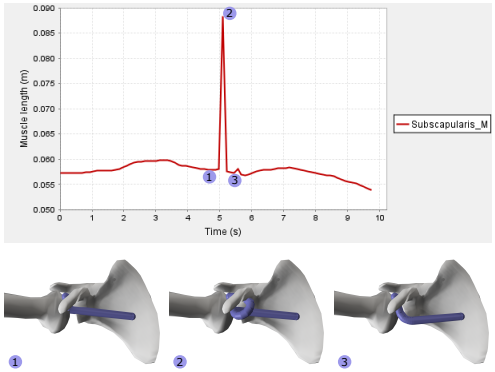

(b) The subscapularis medialis fiber length, with three instances highlighted, showing the muscle wrapping in the model

Fig. 14: Discontinuity of muscles during flexion with a high positional stiffness of the robot